Nanoscale Pinning Effect Evaluated from Deformed Nanobubbles

Teshima, Hideaki
Department of Aeronautics and Astronautics, Kyushu University

Nishiyama, Takashi
Department of Aeronautics and Astronautics, Kyushu University

Takahashi, Koji
Department of Aeronautics and Astronautics, Kyushu University

https://hdl.handle.net/2324/4793619

Nanoscale Pinning Effect Evaluated from Deformed Nanobubbles

Hideaki Teshima[1], Takashi Nishiyama[1,2], Koji Takahashi[1,2]

[1] Department of Aeronautics and Astronautics, Kyushu University, Nishi-Ku, Motooka 744 Fukuoka 819-0395, Japan

[2] International Institute for Carbon-Neutral Energy Research (WPI-I2CNER), Kyushu University, Nishi-Ku, Motooka 744 Fukuoka 819-0395, Japan

ABSTRACT

Classical thermodynamics theory predicts that nanosized bubbles should disappear in a few hundred microseconds. The surprisingly long lifetime and stability of nanobubbles are therefore interesting research subjects. It has been proposed that the stability of nanobubbles arises through pinning of the three-phase contact line, which results from intrinsic nanoscale geometrical and chemical heterogeneities of the substrate. However, a definitive explanation of nanobubble stability is still lacking. In this work, we examined the stability mechanism by introducing a 'pinning force.' We investigated nanobubbles at a highly ordered pyrolytic graphite/pure water interface by peak force quantitative nano-mechanical mapping, and estimated the pinning force and determined its maximum value. We then observed the shape of shrinking nanobubbles. Because the diameter of the shrinking nanobubbles was pinned, the height decreased and the contact angle increased. This phenomenon implies that the stability results from the pinning force, which flattens the bubble through the pinned three-phase contact line and prevents the Laplace

pressure from increasing. The pinning force can also explain the metastability of coalesced nanobubbles, which have two semispherical parts that are joined to form a dumbbell-like shape. The pinning force of the semispherical parts was stronger than that of the joint region. This result demonstrates that the contact line of the semispherical parts is pinned strongly to keep the dumbbell-like shape. Furthermore, we proposed a nanobubble generation mechanism for the solvent-exchange method, and explained why the pinning force of large nanobubbles was not initially at its maximum value, as it was for small nanobubbles.

INTRODUCTION

Many researchers have reported the existence of highly stable solid/liquid interfacial nanobubbles[1–23] both theoretically and experimentally, which defies the thermodynamic prediction that micro- or nanometer-sized bubble should dissolve within a few hundred microseconds[24,25]. Many theories have been proposed to explain nanobubble stability. According to one theory, a contamination layer at the gas/liquid interface of the nanobubbles decreases the surface tension and increases the contact angle, resulting in a decreased Laplace pressure and thus reduced gas outflux[3]. However, subsequent studies have demonstrated this theory to be untenable[26,27]. Another theory holds that nanobubbles are stabilized because diffusive gas outflux caused by the Laplace pressure and gas influx near the three-phase contact line are in equilibrium[22,28,29]. Other investigations have suggested that the stability of the nanobubbles results from the pinning effect on the three-phase contact line, gas oversaturation, or a combination of these factors[17,18,20]. To date, no single stability theory can explain all experimental observations. The development of such a theory is therefore strongly desired.

To explain the contact angle of nanobubbles, line tension has often used[30–32]. Line tension acts as a force per unit length and results from the curvature of the three-phase contact line of the interfacial nanobubbles. According to the modified Young's equation[33], the effect of line tension depends on the radius of the base of the bubble and should be negligible for large

nanobubbles (i.e., with a base radius of greater than 1 μm). However, it was observed that a surface microbubble with a base radius of 4 μm had a substantially larger contact angle than macroscale bubbles[4]. Thus, line tension is not suitable for explaining the different contact angles on the nano- and microscale.

In the present study, we assumed that the contact angle was determined by nanoscale pinning. Thus, we introduced a 'pinning force' acting as a force per unit length on the three-phase contact line, which we estimated qualitatively by observing nanobubbles at a highly ordered pyrolytic graphite (HOPG)/pure liquid interface by peak force quantitative nano-mechanical mapping (PF-QNM).

EXPERIMENT

In this study, the interface between HOPG (SPI-1 grade, 10 mm × 10 mm, Alliance Biosystems Inc., Japan) and pure water was investigated by PF-QNM. An HOPG sample with a thickness of ~0.5 mm was fixed on a stainless-steel Petri dish. Pure water was prepared using a water purifier (RFP742HA, Advantec, Japan) without degassing.

Nanobubbles were generated by the solvent-exchange method[1,2,4,6–8,11,12,14,21,27]. Ethanol was poured into the stainless-steel dish to immerse the HOPG substrate. The ethanol was then displaced by pure water. In this process, local oversaturation conditions are created at the interface between the liquid and the HOPG, resulting in the formation of nanobubbles. The ethanol and pure water were added using a clean disposable pipette to avoid contamination.

Atomic force microscope (AFM) measurements were performed with a Dimension Icon (Bruker AXS) instrument. A ScanAsyst Fluid+ cantilever (tip radius: 2–12 nm; spring constant: 0.7 N m^{-1}) was used. This cantilever is suitable for PF-QNM measurements in liquid. It took approximately 8 minutes to obtain each image.
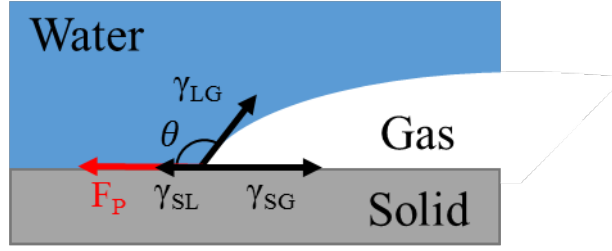
RESULTS AND DISCUSSION

Figure 1. Schematic diagram of the surface tension and pinning force.

A diagram is shown in Figure 1 of the surface tension and pinning force. γ_{SL}, γ_{LG}, and γ_{SG} are surface tension of solid/liquid, liquid/gas, and solid/gas interfaces, respectively. θ is the contact angle and F_P is the pinning force. The pinning force acts on the three-phase contact line in the direction away from the center of the nanobubble, Young's equation is modified accordingly as follows:

$$\cos\theta = \cos\theta_{macro} - \frac{F_P}{\gamma_{LG}} \qquad (1)$$

where θ_{macro} is the macroscopic contact angle. We assume that the force that results from the curvature of three-phase contact line is negligible. Thus, equation (1) can be applied to non-spherical nanobubbles (i.e., coalesced nanobubbles).

Images of the HOPG/water interfacial nanobubbles obtained by PF-QNM measurements are shown in Figure 2. Images were obtained 45, 90, 180, and 230 minutes after the generation of the nanobubbles. PF-QNM measurements were performed with low peak force set-points to avoid influencing the shape of the surface nanobubbles. In general, interfacial nanobubbles on HOPG are stable for a long duration[11,12,15]. We observed that the nanobubbles were deformed when higher set-points of 1.92 and 2.62 nN were used (after 75 and 150 minutes, respectively)[12]. The cause of deformation is the higher set-point, not a time-dependent change[12]. Indeed, no deformation is

observed when comparing the images at 180 and 230 minutes, which were obtained with a low set-point of 462 pN.

From the height information of the nanobubbles obtained through PF-QNM measurements, the contact angles were estimated. By substituting the contact angles into equation (1), the pinning forces acting on the three-phase contact line were calculated. We assumed that θ_{macro} = 89° and γ_{LG} = 72 mN m^{-1} in the calculation[34].
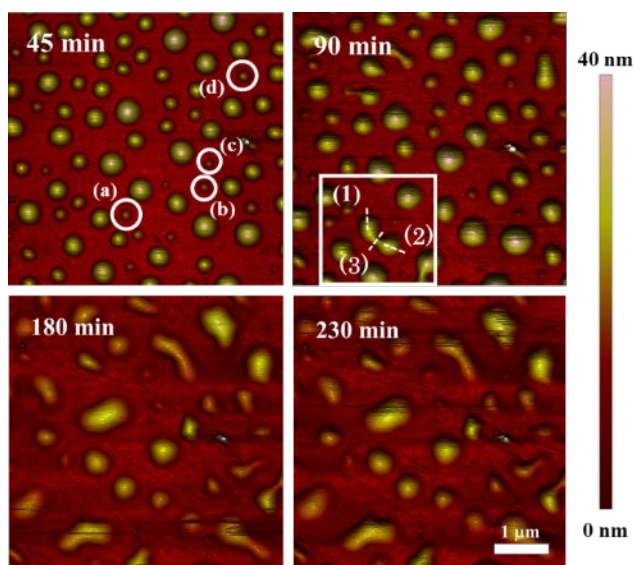

Figure 2. PF-QNM height images (5 μm × 5 μm) of HOPG/water interfacial nanobubbles. The images were obtained 45, 90, 180, and 230 minutes after solvent exchange with low peak force set-points of 903, 770, 462, and 462 pN respectively. The measurements with higher set-points of 1.92 and 2.62 nN were performed after 75 and 150 minutes respectively, and these led the nanobubbles to coalescence. The white circles, marked as (a), (b), (c), and (d), indicate shrinking nanobubbles. The white square indicates a coalesced nanobubble. The dashed lines (1) and (2) show the semispherical parts of the coalesced nanobubble, and dashed line (3) shows the joint region.
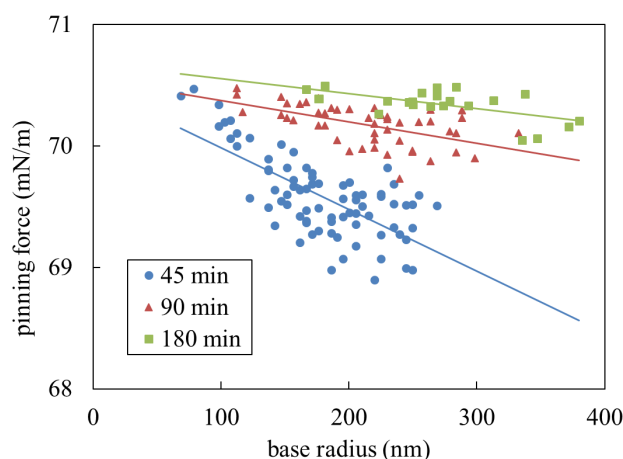
Figure 3. Scatter plot of the pinning force as a function of base radius. The pinning forces were calculated from Eq. (1).

In Figure 3, the pinning force is plotted as a function of base radius for surface nanobubbles obtained after 45, 90, and 180 minutes. The solid lines are linear regressions obtained by least-square fitting. This plot shows a clear dependence of the pinning force on the base radius. However, this dependence became weak as the nanobubbles were flattened (i.e., at 90 and 180 minutes), with the pinning force almost constant at 70.5 mN m^{-1}, which we considered to be the maximum pinning force on the HOPG/pure water interface. The pinning force of the flattened nanobubbles preserves the flat shape.

The pinning effect can result from chemical and/or geometrical heterogeneities[35,36]. Because the surface structure of the HOPG substrate is atomically smooth, local nanoscale heterogeneities can be considered to be negligible. Therefore, the maximum pinning force (i.e., the value that determines the advancing contact angle) should be the same at all locations on the HOPG surface, which is consistent with our results.
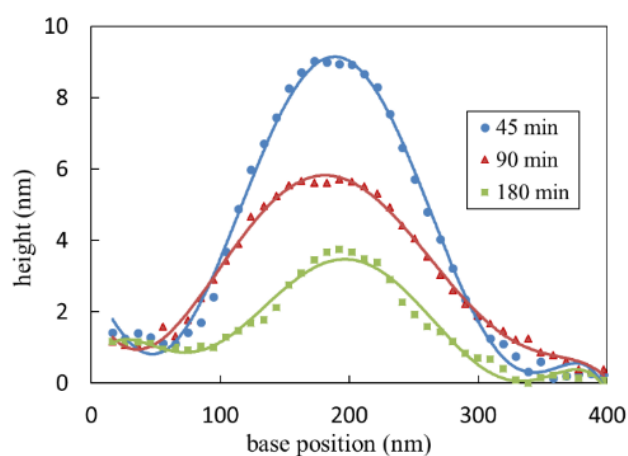
Figure 4. Cross section of the shrinking nanobubble marked as (b) in Figure 2 at different times following solvent exchange. As the nanobubble shrinks, the height markedly decreases and the base radius is almost constant.

Table 1. Contact angle, height, base radius, and radius of curvature of the nanobubbles marked in Figure 2 at different times following solvent exchange. Bubble (c) vanished after 180 minutes.

Nano bubble	Parameter	45 minutes	90 minutes	180 minutes
(a)	Contact angle (°)	173	176	178
	Height (nm)	7.4	3.9	0.7
	Base radius (nm)	117	110	49
	Radius of curvature (nm)	932	1556	1772
(b)	Contact angle (°)	172	175	176
	Height (nm)	7.4	4.7	3.1
	Base radius (nm)	108	108	88
	Radius of curvature (nm)	795	1244	1246
(c)	Contact angle (°)	173	177	-

	Height (nm)	7.4	3.9	-
	Base radius (nm)	103	64	-
	Radius of curvature (nm)	886	1395	-
	Contact angle (°)	171	175	178
	Height (nm)	11.1	5.4	0.8
(d)	Base radius (nm)	137	127	49
	Radius of curvature (nm)	851	1496	1601

The cross sections of an individual shrinking nanobubble at the HOPG/water interface marked by circle (b) in Figure 2 are shown in Figure 4. The solid curves were obtained by least-squares fitting using a sixth-order polynomial. When the nanobubble shrinks, the contact angle increases and the height decreases because the base is pinned. As a result, the radius of curvature increases. The same observation was made for bubbles (a), (c), and (d) in Figure 2, as shown in Table 1. This phenomenon implies that the pinning force increases, causing bubbles to flatten as they shrink. Therefore, the pinning force at the three-phase contact line that flattens nanobubbles at the HOPG/pure water interface prevents the Laplace pressure from driving a gas outflux. As a result, the pinning force increases the radius of curvature and then prevents the nanobubbles from dissolving. In our experiments, the shrinkage of nanobubbles occurred when high peak force set-points were used. However, in other cases (e.g., when nanobubbles shrink as a result of a decrease in the degree of gas saturation in the liquid), the pinning force acting on the three-phase contact line prevents them from dissolving[37].

In addition, some nanobubbles did not shrink after the measurements made with high peak force set-points. We consider that this was because the high peak force set-point measurements caused disturbance, which promoted Ostwald ripening. The shrinkage of small nanobubbles and the growth of large nanobubbles by Ostwald ripening have been previously reported[1,27,38].

When the pinning force acting on the small nanobubbles was lower than the maximum pinning force, the base radius was pinned and the pinning force increased as a result of probing with a higher peak force set-point. Thus, the height decreased and the contact angle increased during net gas diffusion resulting from Ostwald ripening, as shown in Table 1 for nanobubble (a) (as marked in Figure 2) from 45 to 90 minutes. When small nanobubbles with maximum pinning force were probed with a high peak force set-point, the three-phase contact line was temporarily depinned and extended because the pinning force exceeded the limit of the substrate heterogeneity. Subsequently, the three-phase contact line retracted while gas diffused outside the nanobubbles through Ostwald ripening. The three-phase contact line became pinned again when the pinning force decreased below the maximum value. As a result, the base radius decreased, as shown in Table 1 from 90 to 180 minutes. These phenomena have been called constant contact radius mode and stick-slide mode[39–41]. Large nanobubbles were also flattened of the three-phase contact line when a high set-point was used. However, large nanobubbles did not shrink because gas molecules escaping from shrinking nanobubbles diffused into the large nanobubbles through Ostwald ripening.
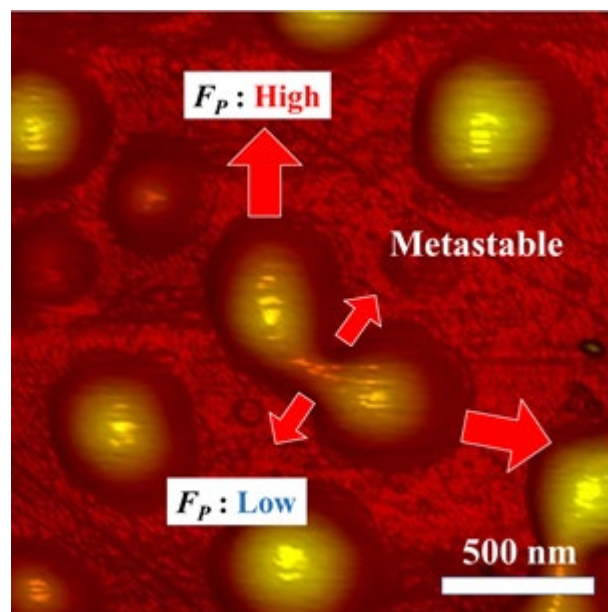
Figure 5. Coalesced nanobubbles marked by the white square in Figure 2. The metastability of coalesced nanobubbles results from large pinning forces on the semispherical parts and a low pinning force on the joint part.
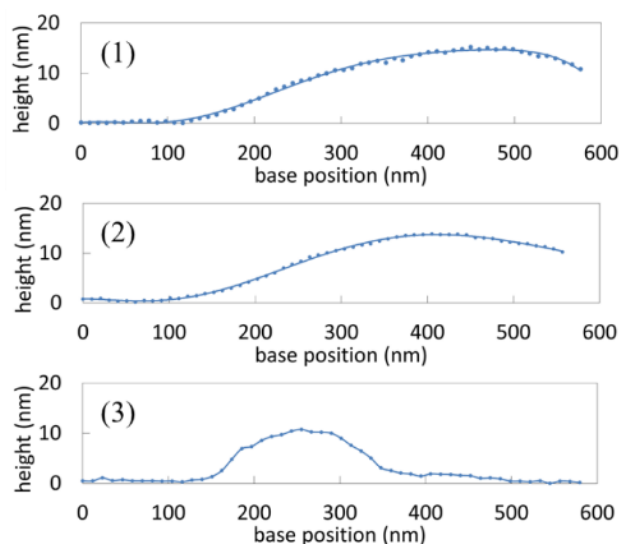

Figure 6. Cross sections of the coalesced nanobubble marked by the white square in Figure 2. Cross sections (1) and (2) show the semispherical parts, and (3) shows the joint part.

Table 2. Contact angle and pinning force of a coalesced nanobubble calculated from the topographical data shown in Figure 5. There is a notable difference between the pinning force and contact angle of the semispherical parts and those of the joint part.

	Contact angle (°)	Pinning force (mN m^{-1})
(1)	175	70.5
(2)	174	70.4
(3)	168	69.4

We now consider a coalesced nanobubble that consists of two semispherical parts and one joint part, similar to the dumbbell-shaped nanobubble in Figure 5. On the macroscale, the

coalesced bubble should immediately become semispherical because of surface tension. However, the coalesced nanobubble retains its dumbbell-like shape for a long time, with similar stability to spherical-cap nanobubbles. From the cross sections shown in Figure 6 of the three parts of the coalesced nanobubble (indicated by the arrows in Figure 2), we estimated the contact angles and pinning forces of each part. The results are shown in Table 2. The contact angle and pinning force of the joint part are substantially smaller than those of the semispherical parts. The other coalesced nanobubbles in Figure 2 exhibited the same tendency.

It has been proposed that the metastability of coalesced nanobubbles requires a very large contact angle hysteresis[12]. However, our results show that the pinning force only acts in the direction of the liquid phase. Therefore, this explanation is probably incorrect. Surface tension reduces the free surface energy by decreasing the surface area. Thus, surface tension causes the coalesced nanobubble to become semispherical through expansion of the joint part. This decreases the contact angle and pinning force of the joint part. However, the larger pinning force of the semispherical parts pins the three-phase contact line and prevents the coalesced nanobubble from assuming a spherical-cap shape. We attribute the metastability of the coalesced nanobubbles to this mechanism.

Interactions between AFM tips and interfacial nanobubbles have been discussed theoretically and experimentally[9,42–45]. Furthermore, nanobubble coalescence resulting from tapping mode (TM)-AFM measurements with high tapping force have been reported[5,46–48]. These studies showed that the coalesced nanobubbles increased in size, but retained a spherical-cap shape. However, in the present study, semispherical nanobubbles coalesced forming a dumbbell-like shape. We attribute the formation of this metastable shape to the different AFM measurement mode used. The cantilever used in TM-AFM oscillates at its resonance frequency, which depends on the type of cantilever and is generally above 100 kHz in liquids. By contrast, in PF-QNM measurements, the cantilever can operate at a lower frequency, down to 2 kHz. In addition, TM-AFM cannot receive feedback from all contact points on the sample surface

because of the high resonance frequency, whereas PF-QNM is able to receive feedback from all contact points. For these reasons, the rate of coalescence when imaging with PF-QNM is lower than that for TM-AFM, which makes it possible to observe dumbbell-like nanobubbles.

As detailed above, the difference in contact angles on the nano- and macroscale at the solid/liquid interface is due to the nanoscale pinning force, which prevents the three-phase contact line from moving and thus prevents the nanobubble from assuming its macroscale shape. As shown in Figure 3, the pinning forces of the nanobubbles with base radii of ~100 nm are approximately 70.5 mN m^{-1}, but nanobubbles with much larger base radii have smaller pinning forces. Thus, the nanoscale pinning force depends on the base radius. The same tendency has been previously reported[4,6,16,23,31,37,46]. If the radius of curvature exclusively depends on the local gas oversaturation and is constant for one particular experiment as predicted previously[20], this dependence of the pinning force on the base radius can be explained by equation (S-1) in supplementary materials. However, we confirmed that the radius of curvature of the interfacial nanobubbles at the HOPG/pure water interface was not constant despite only small variations in the degree of gas saturation (see supplementary material, Figure S-1, S-2, and Equation (S-1)). Some researchers have explained the base radius dependence of the pinning force using a modified Young's equation which includes line tension[30,31,49]. However, we considered the effects of line tension to be negligible in this case. Thus equation (1) does not include a line tension term. If a gas domain on a hydrophobic surface grows from a gas layer to form a surface nanobubble, growth may stop when the pinning force becomes comparable to that from the substrate. The range of the pinning force from the substrate is determined by its roughness and heterogeneity. Therefore, it might be reasonable to expect the pinning force at 45 minutes to have the same maximum value everywhere on the atomically smooth HOPG surface, and that it should not depend on the base radius of the nanobubbles.

To explain this behavior of the pinning force, we propose the following mechanism of nanobubble generation by the solvent-exchange method. As depicted in Figure 7(a), excess gas

molecules appear during solvent exchange and adhere to the solid surface to form gas molecular layers. It has been shown experimentally that gas molecules in pure water adhere and create gas layers at hydrophobic solid/water interfaces[50,51]. We also confirmed that gas molecules adhered to the HOPG surface by conducting PF-QNM measurements without solvent exchange, the results of which are shown in Figure 8. The gas layers may grow into the nanobubbles if solvent exchange is carried out to create the required gas supersaturation.

As the gas layers pile up on the surface, surface tension causes the interface to become curved to reduce the liquid/gas surface area. Consequently, nanoscale gas domains (i.e., nanobubbles) are created. On the three-phase contact line of the nanobubbles, the pinning force acts in the direction of the liquid phase and thus prevents the Laplace pressure from increasing. As a result, nanobubbles at the solid/liquid interface are stable.

We also considered the effect of the base radius. A small nanobubble (with a radius of 100 nm; see Figure 3) is depicted in Figure 7(b). In this case, the pinning force is close to the maximum value before it is probed with a high peak force set-point to decrease the high Laplace pressure to prevent disappearance. There is no volume increase resulting from excess gas molecules. If excess gas molecules diffuse into the small nanobubble, the contact angle decreases and the Laplace pressure increases, which leads to nanobubble dissolution. For a large nanobubble (about 100–300 nm; see Figure 3), as depicted in Figure 7(c), the Laplace pressure is low and the pinning force is much lower than the maximum value. Because of the low Laplace pressure, gas molecules can diffuse into the large nanobubble, further reducing the contact angle and pinning force. Thus, the pinning force depends on the base radius for large nanobubbles.
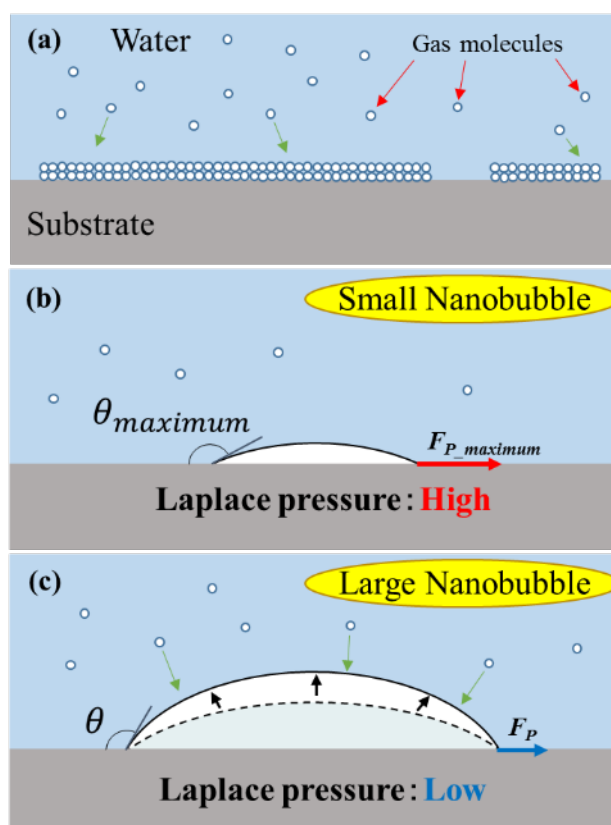
Figure 7. Mechanism of nanobubble generation during solvent exchange. (a) Several layers of gas molecules are formed through solvent exchange. (b) Small nanobubbles have a maximum pinning force, which prevents dissolution owing to the higher Laplace pressure. (c) Large nanobubbles have a weaker pinning force and additional gas can diffuse into the bubble because of the lower Laplace pressure.
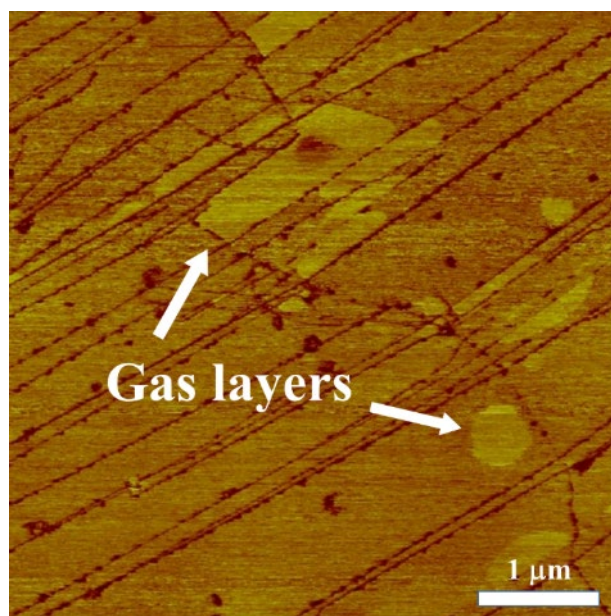
Figure 8. Adhesion image (5 µm × 5 µm) of a HOPG/water interface obtained using PF-QNM. In this experiment, solvent exchange was not carried out. Tiny gas layers indicated by the white arrows were observed on the terraced area between the steps.
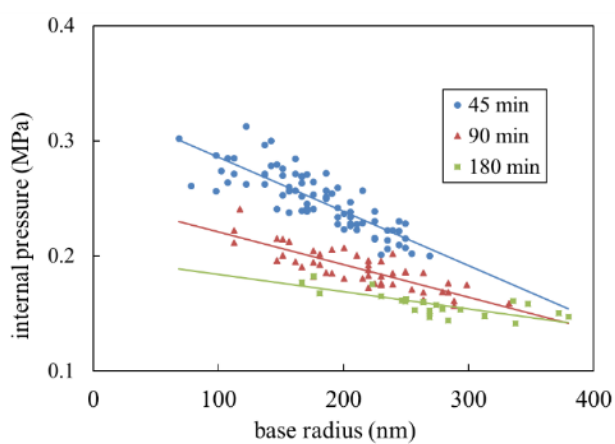

Figure 9. Internal pressure as a function of base radius. Internal pressures were estimated using the Young–Laplace equation.

As shown in Figure 9, nanobubbles flattened in the PF-QNM measurements with higher peak force set-points have lower internal pressure because the pinning force acts to maintain a larger contact angle. In addition, the flattened nanobubbles do not acquire large radii of curvature

through the intake of gas molecules (as illustrated in Figure 7). We assume the reason that new gas molecules do not appear near the HOPG/pure water interface is that water shifts to a lower supersaturated state, which cannot promote nanobubble growth.

CONCLUSIONS

We measured nanobubbles generated at an HOPG/pure water interface using PF-QNM. The pinning force, which we introduced to explain the very large contact angle of the nanobubbles compared with that on the macroscale, was measured using PF-QNM with low peak force set-points. The maximum pinning force was also measured using a high peak force set-point. Our results showed that the pinning force prevents nanobubbles from dissolving by pinning the three-phase contact line. The metastability of coalesced nanobubbles was also explained in terms of differences of the pinning force on the three-phase contact line between the semispherical parts and the joint part. The pinning force at the three-phase contact line depended on the base radius. To explain this behavior, we proposed a mechanism of nanobubble generation through the solvent-exchange method. Specifically, small nanobubbles exhibit a maximum pinning force because of the high Laplace pressure. By contrast, large nanobubbles have low Laplace pressure and can therefore take in additional gas molecules, which reduces the pinning force.

REFERENCES

[1] T. Nishiyama, K. Takahashi, T. Ikuta, Y. Yamada, and Y. Takata, Chemphyschem **17**, 1500 (2016).

[2] C.U. Chan, M. Arora, and C.D. Ohl, Langmuir **31**, 7041 (2015).

[3] W.A. Ducker, Langmuir **25**, 8907 (2009).

[4] C. Xu, S. Peng, G.G. Qiao, V. Gutowski, D. Lohse, and X. Zhang, Soft Matter **10**, 7857 (2014).

[5] B. Bhushan, Y. Wang, and A. Maali, J. Phys. Condens. Matter **20**, 485004 (2008).

[6] L. Zhang, X. Zhang, Y. Zhang, J. Hu, and H. Fang, Soft Matter **6**, 4515 (2010).

[7] X.H. Zhang, N. Maeda, and J. Hu, J. Phys. Chem. B **112**, 13671 (2008).

[8] X.H. Zhang, X.D. Zhang, S.T. Lou, Z.X. Zhang, J.L. Sun, and J. Hu, Langmuir **20**, 3813 (2004).

[9] B. Zhao, Y. Song, S. Wang, B. Dai, L. Zhang, Y. Dong, J. Lü, and J. Hu, Soft Matter **9**, 8837 (2013).

[10] C. Yang, Y. Lu, and I. Hwang, J. Phys. Condens. Matter **25**, 184010 (2013).

[11] S. Yang, E.S. Kooij, B. Poelsema, D. Lohse, and H.J.W. Zandvliet, EPL (Europhysics Lett. **81**, 64006 (2008).

[12] T. Nishiyama, Y. Yamada, T. Ikuta, K. Takahashi, and Y. Takata, Langmuir **31**, 982 (2015).

[13] K. Kikuchi, S. Nagata, Y. Tanaka, Y. Saihara, and Z. Ogumi, J. Electroanal. Chem. **600**, 303 (2007).

[14] B.M. Borkent, S.M. Dammer, H. Schonherr, G.J. Vancso, and D. Lohse, SOCAR Proc. **98**, 204502 (2007).

[15] S. Yang, P. Tsai, E.S. Kooij, A. Prosperetti, H.J.W. Zandvliet, and D. Lohse, Langmuir **25**, 1466 (2009).

[16] X. Wang, B. Zhao, W. Ma, Y. Wang, X. Gao, R. Tai, X. Zhou, and L. Zhang, ChemPhysChem **16**, 1003 (2015).

[17] Y. Liu, J. Wang, X. Zhang, and W. Wang, J. Chem. Phys. **140**, 54705 (2014).

[18] Y. Liu and X. Zhang, J. Chem. Phys. **138**, 14706 (2013).

[19] Y. Liu and X. Zhang, J. Chem. Phys. **141**, 134702 (2014).

[20] D. Lohse and X. Zhang, Phys. Rev. E **91**, 31003 (2015).

[21] S.-T. Lou, Z.-Q. Ouyang, Y. Zhang, X.-J. Li, J. Hu, M.-Q. Li, and F.-J. Yang, J. Vac. Sci. Technol. B Microelectron. Nanom. Struct. **18**, 2573 (2000).

[22] M.P. Brenner and D. Lohse, Phys. Rev. Lett. **101**, 214505 (2008).

[23] B. Song, K. Chen, and M. Schmittel, Langmuir (2016).

[24] P.S. Epstein and M.S. Plesset, J. Chem. Phys. **18**, 1505 (1950).

[25] S. Ljunggren and J.C. Eriksson, Colloids Surfaces A Physicochem. Eng. Asp. **129**–**130**, 151 (1997).

[26] X. Zhang, M.H. Uddin, H. Yang, G. Toikka, W. Ducker, and N. Maeda, Langmuir **28**, 10471 (2012).

[27] S.R. German, X. Wu, H. An, V.S.J. Craig, T.L. Mega, X. Zhang, R. Corporation, U. States, B. Engineering, A. Mathematics, P. Sciences, and C. Act, ACS Nano **8**, 6193 (2014).

[28] N.D. Petsev, M.S. Shell, and L.G. Leal, Phys. Rev. E - Stat. Nonlinear, Soft Matter Phys. **88**, 10402 (2013).

[29] K. Yasui, T. Tuziuti, W. Kanematsu, and K. Kato, Phys. Rev. E **91**, 33008 (2015).

[30] J. Yang, J. Duan, D. Fornasiero, and J. Ralston, J. Phys. Chem. B **107**, 6139 (2003).

[31] N. Kameda and S. Nakabayashi, Chem. Phys. Lett. **461**, 122 (2008).

[32] N. Kameda, N. Sogoshi, and S. Nakabayashi, Surf. Sci. **602**, 1579 (2008).

[33] J. Drelich and J.D. Miller, Colloids and Surfaces **69**, 35 (1992).

[34] R. Raj, S.C. Maroo, and E.N. Wang, Nano Lett. **13**, 1509 (2013).

[35] P.G. De Gennes, Rev. Mod. Phys. **57**, 827 (1985).

[36] G. Shen, X.-H. Zhang, Y. Ming, L. Zhang, Y. Zhang, and J. Hu, J. Phys. Chem. C Lett. **112**, 4029 (2008).

[37] X. Zhang, D.Y.C. Chan, D. Wang, and N. Maeda, Langmuir **29**, 1017 (2013).

[38] D. Shin, J.B. Park, Y. Kim, S.J. Kim, J.H. Kang, B. Lee, S.-P. Cho, B.H. Hong, and K.S. Novoselov, Nat. Commun. **6**, 6068 (2015).

[39] E. Dietrich, E.S. Kooij, X. Zhang, H.J.W. Zandvliet, and D. Lohse, Langmuir **31**, 4696 (2015).

[40] X. Zhang, J. Wang, L. Bao, E. Dietrich, R.C. a van der Veen, S. Peng, J. Friend, H.J.W. Zandvliet, L. Yeo, and D. Lohse, Soft Matter **11**, 1889 (2015).

[41] J.M. Stauber, S.K. Wilson, B.R. Duffy, and K. Sefiane, J. Fluid Mech. **744**, R2 (2014).

[42] Z. Guo, Y. Liu, Q. Xiao, H. Schönherr, and X. Zhang, Langmuir **32**, 751 (2016).

[43] W. Walczyk, N. Hain, and H. Schönherr, Soft Matter **10**, 5945 (2014).

[44] W. Walczyk and P.M. Sch, J Phys Condens Matter **25**, 184005 (2013).

[45] Y. Wang, H. Wang, S. Bi, and B. Guo, Sci. Rep. **6**, 30021 (2016).

[46] A.C. Simonsen, P.L. Hansen, and B. Klösgen, J. Colloid Interface Sci. **273**, 291 (2004).

[47] A. Agrawal, J. Park, D.Y. Ryu, P.T. Hammond, T.P. Russell, and G.H. McKinley, Nano Lett. **5**, 1751 (2005).

[48] M.A. Hampton and A. V. Nguyen, Adv. Colloid Interface Sci. **154**, 30 (2010).

[49] N. Ishida, T. Inoue, M. Miyahara, and K. Higashitani, Langmuir **16**, 6377 (2000).

[50] Y.H. Lu, C.W. Yang, and I.S. Hwang, Langmuir **28**, 12691 (2012).

[51] C.-K. Fang, H.-C. Ko, C.-W. Yang, Y.-H. Lu, and I.-S. Hwang, Sci. Rep. **6**, 24651 (2016).